ACADEMIC PRESS

Available online at www.sciencedirect.com

SCIENCE DIRECT®

Journal of Magnetic Resonance 160 (2003) 40–46

JMR Journal of Magnetic Resonance

www.elsevier.com/locate/jmr

Correlation of fast and slow chemical shift spinning sideband patterns under fast magic-angle spinning

Bénédicte Eléna, Sabine Hediger, and Lyndon Emsley*

Laboratoire de Stéréochimie et des Interactions Moléculaires, UMR 5532, CNRS/ENS Lyon, Laboratoire de Recherche Conventionné du CEA (23 V), Ecole Normale Supérieure de Lyon, 46 allée d'Italie, 69364 Lyon, France

Received 28 May 2002; revised 5 August 2002

Abstract

A new two-dimensional solid-state NMR experiment, which correlates slow and fast chemical shift anisotropy sideband patterns is proposed. The experiment, dubbed ROSES, is performed under fast magic-angle spinning and leads to an isotropic spectrum in the directly detected ω_2 dimension. In the evolution dimension ω_1, the isotropic chemical shift is reduced by a factor S, and spinning sidebands are observed spaced by a scaled effective spinning speed ω_R/S. These spinning sidebands patterns are not identical to those observed with standard slow magic-angle spinning experiments. Chemical shift anisotropy parameters can be accurately extracted with standard methods from these spinning sideband patterns. The experiment is demonstrated with carbon-13 experiments on powdered samples of a dipeptide and a cyclic undecapeptide, cyclosporin-A.

Keywords: Solid-state NMR; MAS; Chemical shift anisotropy; Scaling; Spinning sidebands

1. Introduction

Magic-angle spinning (MAS), usually in combination with cross-polarization, has become the central method for the study of powder samples in solid-state NMR [1–3]. The chemical shift anisotropy (CSA) is a powerful probe of molecular structure and dynamics [4–7], and its measurement should lead to advances in areas as diverse as inorganic materials and structural biology. Under fast rotation at the magic angle, all of the second rank interactions, such as the chemical shift anisotropy, are effectively averaged to zero and high-resolution spectra can be obtained with high sensitivity for magnetically dilute spins, such as carbon-13 or nitrogen-15. In a slower spinning regime, when the magic-angle spinning frequency ω_R is less than the magnitude of the CSA, spinning sideband patterns are observed [8]. These sideband patterns consist of a series of resonances centered on the isotropic chemical shift and spaced by ω_R. The intensity distribution of the spinning sidebands is characteristic of the CSA tensor, and the distribution is widely used to experimentally determine CSA parameters [9,10]. Indeed, the spinning sideband patterns can provide a more accurate determination of the CSA parameters than a non-spinning spectrum [11].

However, since typical organic compounds present a multitude of chemically inequivalent sites, spectral overlap often prevents the extraction of CSA parameters from either static or slow spinning spectra. To overcome this drawback a series of two-dimensional (2D) experiments have been proposed, the common principle of these experiments being to use a second dimension to separate overlapping resonances according to their isotropic chemical shift.

A first class of experiments, performed at low MAS spinning speeds, yields spectra showing spinning sidebands in the directly detected ω_2 dimension, with either an isotropic (sideband free) spectrum being obtained in the indirect ω_1 dimension, in the case of MAT type experiments [12–14], or a spectrum separated by the sideband order in the case of PASS-type techniques [15–17]. These experiments are widely used to

* Corresponding author. Fax: +33-4-72-72-8483.
E-mail address: lyndon.emsley@ens-lyon.fr (L. Emsley).

1090-7807/02/$ - see front matter © 2002 Elsevier Science (USA). All rights reserved.
PII: S1090-7807(02)00037-X

determine CSAs for numerous nuclei, but they become technically difficult to implement for small CSAs, since for accurate measurements they require MAS spinning speeds substantially smaller than the chemical shift anisotropies.

A second class of experiments involves different approaches to reintroducing CSAs under fast MAS. These experiments yield isotropic spectra in the directly detected dimension (ω_2). One class of such experiments includes a variety of methods for recoupling the anisotropy, leading to static-like scaled powder patterns [18–22], or peaks at the principal values of the CSA tensor [23] in the indirect dimension (ω_1). A second approach involves 2D experiments which yield sideband patterns in the indirect dimension where the spinning sidebands appear at some fraction of the actual spinning speed [24–26]. Notably, in this category Crockford et al. [26] recently introduced a sequence based on a 2D PASS approach which correlates fast and slow CSA spinning sideband patterns. Sideband intensities observed in the ω_1 dimension are identical to those obtained in a standard MAS spectrum acquired at a spinning speed ω_R/N, where the 'reduction factor' N can be as large as 8.

In this paper, we develop a new approach for 2D fast-slow spinning correlation. In terms of the discussion above, our approach is most closely related to the earlier ideas of Kolbert et al. [24] and Gullion [25]. The experiment is performed under fast MAS and yields fast spinning isotropic spectra in the ω_2 dimension, with spinning sidebands in the indirect dimension appearing at multiples of an apparent spinning speed ω_R/S, where the "scaling factor" S of the sequence is easily varied, and is in theory not limited. The experiment yields modified sideband patterns in ω_1, which are not identical to "standard" CSA sideband patterns, but which can straightforwardly be used to determine the CSA parameters for each resolved site. Carbon-13 experiments involving spinning speed scaling factors up to 30 have been successfully performed.

2. Pulse scheme

The pulse sequence suitable for the carbon-13 fast-slow correlation experiment is shown in Fig. 1. After cross-polarization from protons, the carbon-13 magnetization evolves during t_1 under a periodic rotor-synchronized pulse sequence. Each period T_S of this sequence can be divided into two parts: a delay τ, followed by a rotor period T_R which contains two π-pulses spaced by half a rotor period: the first π-pulse is located in the middle of this T_R period while the second one occurs at the end. The length of the τ period determines the spinning speed scaling factor of the sequence, which as will be shown below, is given by $S = (T_R + \tau)/\tau$,

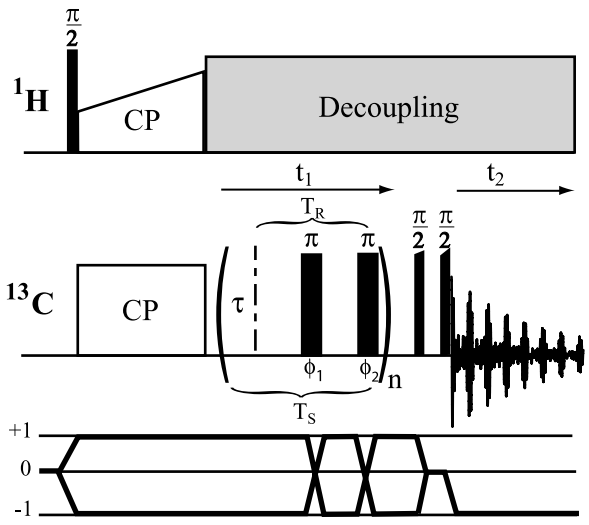

Fig. 1. Pulse sequence and coherence transfer pathways for the ROSES experiment. The repeating unit T_S during the evolution period consists in the free adjustable delay τ followed by one rotor period T_R containing two π-pulses. The phases ϕ_1 and ϕ_2 of the pi pulses are alternated in order to reduce off-resonance effects. The pulses programs and phase cycle used in this work are available from our website: http://www.ens-lyon.fr/STIM/NMR.

yielding spinning sidebands on the ω_1 dimension of the corresponding spectrum spaced by ω_R/S. We dub this experiment ROSES, for Results in the Observation of Slower Effective Spinning.

3. Theory

For the theoretical development of the ROSES sequence, we choose to follow the conventions and notations used by Antzutkin in [27]. Let us first describe the chemical shift Hamiltonian using the irreducible spherical tensor representation [28]. Considering a single spin $I = 1/2$ evolving only under the Zeeman and chemical shift interactions, the rotating-frame Hamiltonian (with respect to Zeeman interaction) under MAS is time-dependent and can be written for a single orientation as

$$\mathscr{H}(\Omega_{PL}(t)) = \left[\omega_{iso} + A^{L}_{20}(t)\right] I_z = \omega(\Omega_{PL}(t)) I_z \qquad (1)$$

with ω_{iso} the isotropic-shift frequency in the rotating frame, Ω_{PL} the set of Euler angles describing the orientation of the principle axes of the CSA tensor with respect to the laboratory frame, and $A^{L}_{20}(t)$ the time-dependent anisotropic part of the CSA in the laboratory frame (index L). The frequency $\omega(\Omega_{PL}(t))$ is obtained by the successive transformations from the principal axis system P of the CSA to the rotor-fixed frame R (P $\rightarrow$ R) and from the rotor-fixed frame R to

the laboratory frame L (R → L). Using elements of the Wigner rotation matrices of 2nd rank $D^{(2)}_{mn}(\Omega)$, one obtains

$$\begin{aligned}\omega(\Omega_{\mathrm{PL}}(t)) &= \omega_{\mathrm{iso}} + \sum_{m=-2}^{2} A^{\mathrm{R}}_{2m} D^{(2)}_{m0}(\Omega_{\mathrm{RL}}(t)) \\ &= \omega_{\mathrm{iso}} + \sum_{m=-2}^{2}\sum_{m'=-2}^{2} A^{\mathrm{P}}_{2m'} D^{(2)}_{m'm}(\Omega_{\mathrm{PR}}) D^{(2)}_{m0}(\Omega_{\mathrm{RL}}(t))\end{aligned} \tag{2}$$

with $\Omega_{\mathrm{RL}}(t) = \{\alpha^0_{\mathrm{RL}} - \omega_{\mathrm{R}} t, \theta_m, 0\}$ the set of Euler angles describing the MAS rotation with a spinning frequency ω_{R} about an axis tilted by the magic angle $\theta_m = \arccos(1/\sqrt{3})$ with respect to the z-axis of the laboratory frame. α^0_{RL} is the initial phase of the rotor and can be chosen arbitrarily. The spherical spatial tensors of the CSA in the principal axis system are given by

$$\begin{aligned}&A^{\mathrm{P}}_{20} = -\omega_0\left(\sigma^{\mathrm{P}}_{zz} - \sigma_{\mathrm{iso}}\right) = \omega^{\mathrm{P}}_{\mathrm{aniso}}, \quad A^{\mathrm{P}}_{2\pm1} = 0, \\ &A^{\mathrm{P}}_{2\pm2} = -\frac{\eta}{\sqrt{6}} A^{\mathrm{P}}_{20}\end{aligned} \tag{3}$$

using the usual convention for ordering the chemical shift principal values $|\sigma^{\mathrm{P}}_{zz} - \sigma_{\mathrm{iso}}| \geqslant |\sigma^{\mathrm{P}}_{xx} - \sigma_{\mathrm{iso}}| \geqslant |\sigma^{\mathrm{P}}_{yy} - \sigma_{\mathrm{iso}}|$. The isotropic shift σ_{iso}, the anisotropy δ, and the asymmetry parameter η are defined as

$$\begin{aligned}&\sigma_{\mathrm{iso}} = \frac{1}{3}\left(\sigma^{\mathrm{P}}_{xx} + \sigma^{\mathrm{P}}_{yy} + \sigma^{\mathrm{P}}_{zz}\right), \quad \delta = \sigma^{\mathrm{P}}_{zz} - \sigma_{\mathrm{iso}}, \\ &\eta = \frac{\sigma^{\mathrm{P}}_{yy} - \sigma^{\mathrm{P}}_{xx}}{\sigma^{\mathrm{P}}_{zz} - \sigma_{\mathrm{iso}}}.\end{aligned} \tag{4}$$

Expanding the Wigner rotation matrix $D^{(2)}_{m0}(\Omega_{\mathrm{RL}}(t))$ of Eq. (2) with the reduced Wigner rotation matrix elements $d^{(2)}_{mn}(\beta)$, $\omega(\Omega_{\mathrm{PL}}(t))$ can be expressed as a Fourier series

$$\begin{aligned}\omega(\Omega_{\mathrm{PL}}(t)) &= \omega_{\mathrm{iso}} + \sum_{m=-2}^{2} \omega^{(m)}(\Omega_{\mathrm{PR}}) \exp(\mathrm{im}\,\omega_{\mathrm{R}} t) \\ &= \omega(t; \Omega_{\mathrm{PR}})\end{aligned} \tag{5}$$

with the Fourier components

$$\begin{aligned}\omega^{(m)}(\Omega_{\mathrm{PR}}) = &\sum_{m'=-2}^{2} A^{\mathrm{P}}_{2m'} D^{(2)}_{m'm}(\Omega_{\mathrm{PR}}) d^{(2)}_{m0}(\theta_m) \\ &\times \exp(-\mathrm{im}\,\alpha^0_{\mathrm{RL}}).\end{aligned} \tag{6}$$

We can now define for one crystallite orientation Ω_{PR} the total propagator $U(T_{\mathrm{S}}, 0; \Omega_{\mathrm{PR}})$ over one T_{S} period under the ROSES sequence

$$\begin{aligned}U(T_{\mathrm{S}}, 0; \Omega_{\mathrm{PR}}) = &U(\pi_x) U\left(T_{\mathrm{S}}, \frac{T_{\mathrm{R}}}{2} + \tau; \Omega_{\mathrm{PR}}\right) U^{\dagger}(\pi_x) \\ &\times U\left(\frac{T_{\mathrm{R}}}{2} + \tau, 0; \Omega_{\mathrm{PR}}\right),\end{aligned} \tag{7}$$

where $U(\pi_x) = \exp(-\mathrm{i}\pi I_x)$ is the propagator of an ideal π pulse of phase x and $U(t_{\mathrm{b}}, t_{\mathrm{a}}; \Omega_{\mathrm{PR}}) = \exp\{-\mathrm{i}\Phi(t_{\mathrm{b}}, t_{\mathrm{a}}; \Omega_{\mathrm{PR}}) I_z\}$ the free evolution propagator under the inhomogeneous Hamiltonian of Eq. (1). The integrated phase function is defined as:

$$\Phi(t_{\mathrm{b}}, t_{\mathrm{a}}; \Omega_{\mathrm{PR}}) = \int_{t_{\mathrm{a}}}^{t_{\mathrm{b}}} \omega(t; \Omega_{\mathrm{PR}})\, \mathrm{d}t. \tag{8}$$

Using a property of exponential operators [29],

$$U(\pi_x) U(t_{\mathrm{b}}, t_{\mathrm{a}}) U^{\dagger}(\pi_x) = U^{\dagger}(t_{\mathrm{b}}, t_{\mathrm{a}}), \tag{9}$$

the propagator of Eq. (7) can be rewritten:

$$\begin{aligned}U(T_{\mathrm{S}}, 0; \Omega_{\mathrm{PR}}) &= U^{\dagger}\left(T_{\mathrm{S}}, \frac{T_{\mathrm{R}}}{2} + \tau; \Omega_{\mathrm{PR}}\right) U\left(\frac{T_{\mathrm{R}}}{2} + \tau, 0; \Omega_{\mathrm{PR}}\right) \\ &= \exp\left\{-\mathrm{i}\left[-\Phi\left(T_{\mathrm{S}}, \frac{T_{\mathrm{R}}}{2} + \tau; \Omega_{\mathrm{PR}}\right)\right.\right. \\ &\quad \left.\left. + \Phi\left(\frac{T_{\mathrm{R}}}{2} + \tau, 0; \Omega_{\mathrm{PR}}\right)\right] I_z\right\} \\ &= \exp\{-\mathrm{i}\Phi_{\mathrm{ROSES}}(T_{\mathrm{S}}, 0; \Omega_{\mathrm{PR}}) I_z\}.\end{aligned} \tag{10}$$

The overall phase function of the ROSES sequence, $\Phi_{\mathrm{ROSES}}(T_{\mathrm{S}}, 0; \Omega_{\mathrm{PR}})$, can be integrated using Eq. (5)

$$\begin{aligned}\Phi_{\mathrm{ROSES}}(T_{\mathrm{S}}, 0; \Omega_{\mathrm{PR}}) = &\omega_{\mathrm{iso}}\tau + 2\xi\left(\frac{T_{\mathrm{R}}}{2} + \tau; \Omega_{\mathrm{PR}}\right) \\ &- \xi(T_{\mathrm{R}} + \tau; \Omega_{\mathrm{PR}}) - \xi(0; \Omega_{\mathrm{PR}})\end{aligned} \tag{11}$$

with the real function $\xi(t; \Omega_{\mathrm{PR}})$ defined as

$$\begin{aligned}\xi(t; \Omega_{\mathrm{PR}}) &= \sum_{\substack{m=-2 \\ m\neq 0}}^{2} \frac{\omega^{(m)}(\Omega_{\mathrm{PR}}) \exp(\mathrm{im}\,\omega_{\mathrm{R}} t)}{\mathrm{im}\,\omega_{\mathrm{R}}} \\ &= \sum_{\substack{m=-2 \\ m\neq 0}}^{2} \xi^{(m)}(t; \Omega_{\mathrm{PR}}).\end{aligned} \tag{12}$$

We can now analyze the different contributions to $\Phi_{\mathrm{ROSES}}(T_{\mathrm{S}}, 0; \Omega_{\mathrm{PR}})$ according to their time dependence, considering $T_{\mathrm{R}} = 2\pi/\omega_{\mathrm{R}}$:

$$\Phi^{(0)}_{\mathrm{ROSES}}(T_{\mathrm{S}}, 0; \Omega_{\mathrm{PR}}) = \omega_{\mathrm{iso}}\tau = \frac{\omega_{\mathrm{iso}}}{S} T_{\mathrm{S}}, \tag{13a}$$

$$\begin{aligned}\Phi^{(\pm1)}_{\mathrm{ROSES}}(T_{\mathrm{S}}, 0; \Omega_{\mathrm{PR}}) &= -3\xi^{(\pm1)}(\tau; \Omega_{\mathrm{PR}}) \\ &\quad - \xi^{(\pm1)}(0; \Omega_{\mathrm{PR}}) \\ &= -3\xi^{(\pm1)}\left(\frac{T_{\mathrm{S}}}{S}; \Omega_{\mathrm{PR}}\right) \\ &\quad - \xi^{(\pm1)}(0; \Omega_{\mathrm{PR}}),\end{aligned} \tag{13b}$$

$$\begin{aligned}\Phi^{(\pm2)}_{\mathrm{ROSES}}(T_{\mathrm{S}}, 0; \Omega_{\mathrm{PR}}) &= \xi^{(\pm2)}(\tau; \Omega_{\mathrm{PR}}) - \xi^{(\pm2)}(0; \Omega_{\mathrm{PR}}) \\ &= \xi^{(\pm2)}\left(\frac{T_{\mathrm{S}}}{S}; \Omega_{\mathrm{PR}}\right) \\ &\quad - \xi^{(\pm2)}(0; \Omega_{\mathrm{PR}})\end{aligned} \tag{13c}$$

with the scaling factor $S = (T_R + \tau)/\tau = T_S/\tau$. As can be seen from Eq. (13a), the isotropic chemical shift evolves only during the τ period. Thus the observed isotropic chemical shift over one period of the ROSES sequence (during the indirect detection period t_1) is ω_{iso}/S, the isotropic chemical shift scaled by the factor S. Analogously the terms oscillating at ω_R and $2\omega_R$ in Eqs. (13b) and (13c) are as well only be effectively "active" during the τ period [30]. Again, this can be interpreted as a scaling of the rotation frequency ω_R by the scaling factor S in the time-dependence of the Fourier components $\xi^{(m)}(t, \Omega_{PR})$ in Eq. (12). Therefore, spinning sidebands under ROSES will appear separated by the scaled rotation frequency ω_R/S. However, the intensities of the spinning sidebands will differ from those found for a normal one-dimensional (1D) spectrum recorded at the equivalent slower spinning speed, as the integrated phase function components of Eqs. (13a) and (13b) under ROSES are different from the components found for free evolution. Nevertheless, the spinning sideband pattern under ROSES still depends on the whole CSA tensor and allows therefore the measurement of the anisotropy and asymmetry parameters.

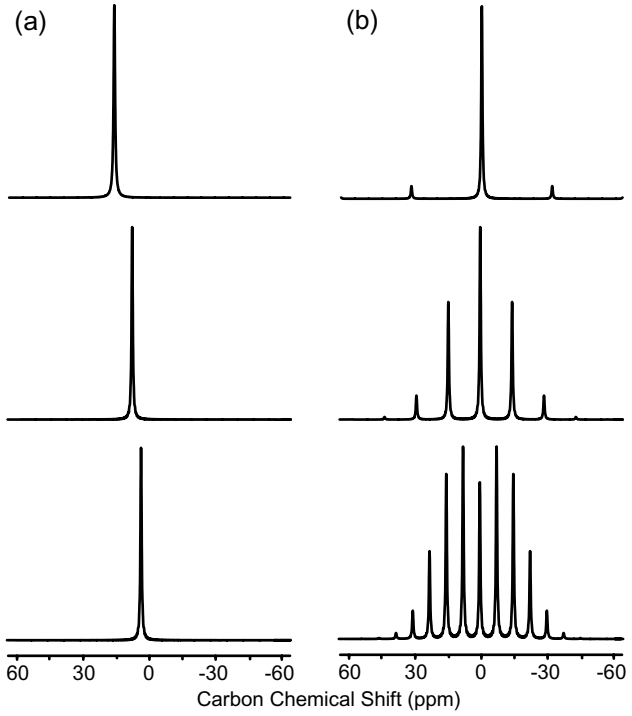

Fig. 2. Simulations of the effect of the ROSES sequence on (a) a pure isotropic ^{13}C chemical shift of $\sigma_{iso} = 80$ ppm, (b) a CSA of $\delta = 60$ ppm with no isotropic chemical shift and $\eta = 1$. A spinning speed of 20 kHz was used. The delay τ was set to obtain respective scaling factors of 5 (top), 11 (middle), and 21 (bottom). In (a), the isotropic chemical shift is scaled as expected with the scaling factor given above. Spinning sidebands, spaced with the effective spinning speeds of 4 kHz, 1818 Hz, and 952 Hz respectively, are observed (b). The simulations were performed with the program Simpson [31].

4. Simulations

Fig. 2a shows simulations of the effect of the ROSES sequence on a single spin with a pure isotropic chemical shift ($\delta = 0$) at a spinning speed of 20 kHz, with various applied scaling factors. The numerical simulations were done with SIMPSON software [31] using standard methods [32]. The π-pulses were assumed to be ideal. As expected, the isotropic shift σ_{iso} is scaled down by a factor S, so that resonance occurs at frequency σ_{iso}/S. This scaling of the isotropic chemical shift in the indirect dimension is in practice particularly useful for the 2D ROSES experiment, where the spectral width ω_S in the evolution dimension ω_1 is defined by $\omega_S = 1/(T_R + \tau)$, which means that it is limited by the actual spinning speed ($\omega_S < \omega_R$). The scaling of the isotropic chemical shift leads in the indirect dimension to a translation of the spinning sideband patterns for each site towards the center of the spectrum. It is then always possible, using large scaling factors, to have all the resonances within the spectral width. Fig. 2b shows simulations under the same conditions as Fig. 2a, for a non-zero symmetric CSA ($\eta = 1$) with zero isotropic shift. As predicted, for each of the different scaling factors S, spinning sidebands appear spaced by the frequency ω_R/S. This clearly confirms that modifying the scaling factor of the ROSES experiment scales down the apparent spinning speed, without affecting the apparent amplitude of the anisotropy. Additionally, this also implies that it is not possible to measure CSAs larger than the actual spinning speed using ROSES, as the spinning sideband

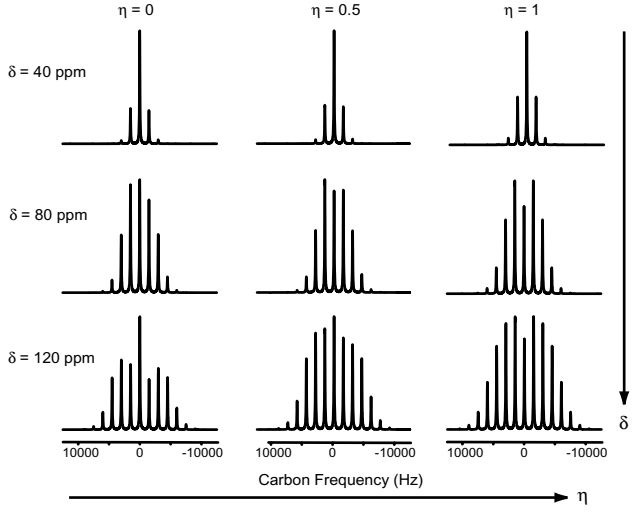

Fig. 3. Simulations showing the behaviour of the ROSES sequence as a function of δ and η. The actual spinning speed was set to 15 kHz, and a ROSES scaling factor of 17.7 was used. Spinning sidebands appear at multiples of the expected scaled spinning speed of 849 Hz. The evolution of CSA spinning sideband patterns is shown. Carbon frequencies are given in unscaled units.

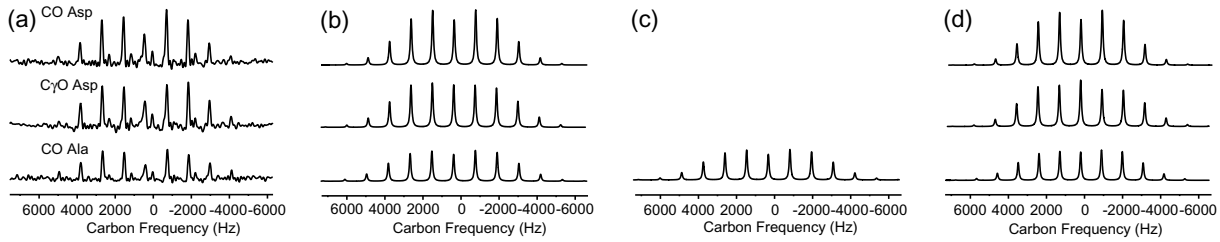

Fig. 4. (a) F_1 traces at the carbonyl resonances of a powder sample of L-alanyl-L-aspartic acid extracted from a 2D ROSES spectrum, (b) corresponding best fits from experiment, (c) reference data from the literature [35], and (d) simulations using CSA parameters obtained previously from a MAT spectrum acquired at 2 kHz MAS. The spinning speed was set to 20 kHz. Thirty-two scans were accumulated for each of the 256 points in the t_1 dimension. The repetition time was 3 s. The τ-delay during the evolution period t_1 was set to 3 μs to obtain a ROSES scaling factor of 17.7, corresponding to an effective scaled spinning speed of 1132 Hz. Composite $(90°_{\alpha} - 270°_{\alpha+90°} - 90°_{\alpha})$ pulses were used for the π-pulses during t_1 evolution. CSA parameters for (b), (c) and (d) are given in Table 1.

patterns would not then fit within the ω_1 spectral width. In most cases, this limitation does not affect the study of nuclei with moderate CSAs, such as carbon-13. In any case, as mentioned in the introduction, our objective is to provide an experiment suited to the measurement of small CSAs.

Fig. 3 presents the dependence of ROSES CSA sidebands patterns on the chemical shift anisotropy δ and the asymmetry η. The simulations were performed with a spinning speed of 15 kHz and a scaling factor of 17.7. Both parameters δ and η clearly affect the relative amplitudes of the observed spinning sidebands. As for a standard magic-angle spinning experiment [11], CSA parameters can therefore be reliably extracted from ROSES spinning sideband patterns.

5. Experimental

Experiments were performed on a Bruker DSX 500 spectrometer (125.7 MHz carbon-13 resonance frequency), using a 2.5-mm double-resonance CPMAS probe. Figs. 4 and 5 show ω_1 slices taken through a carbon-13 2D ROSES spectrum on a powdered sample of L-alanyl-L-aspartic acid. Due to the large number of π-pulses applied during the evolution period, the ROSES experiment is quite sensitive to off-resonance effects. Composite π-pulses $(90°_{\alpha} - 270°_{\alpha+90°} - 90°_{\alpha})$ were used [33], along with phase reversal for the two π-pulses in each t_1 increment, in order to reduce sensitivity to off-resonance effects. The carbon-13 RF field strength was set to 120 kHz, and no further phase cycling was used for the π-pulses. Quadrature detection in ω_1 was achieved using the States method [34].

Fig. 4a shows slices taken from the experimental ROSES spectrum for the three carbonyl resonances in the molecule. Fig. 4b shows simulations corresponding to the "best fit" of these data obtained by iteratively comparing the spectra manually with simulations. The parameters for the anisotropy of the three sites obtained

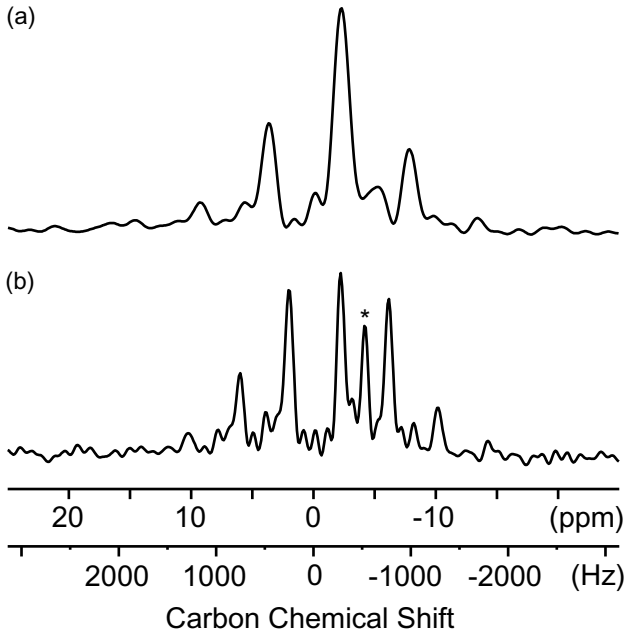

Fig. 5. F_1 traces extracted from 2D ROSES spectra, corresponding to the CH_3 resonance (C_β) of the alanine residue of a powder sample of L-alanyl-L-aspartic acid. Both spectra were acquired with a 15 kHz spinning speed and with ROSES scaling factors of (a) 21, and (b) 29.6, corresponding to effective spinning speeds of 714 and 507 Hz, respectively. Thirty-two scans were acquired for each of the 256 points in the t_1 dimension, using a repetition time of 3.2 s. Composite $(90°_{\alpha} - 270°_{\alpha+90°} - 90°_{\alpha})$ pulses were used for the π-pulses during t_1 evolution. Artefacts are indicated by asterisks.

in this way are given in Table 1, where they are compared to both a reference value available in the literature [35] for the CO-Ala site, and to the results obtained from fits to an experimental 2D MAT spectrum obtained with a 2 kHz spinning speed for all three sites. These comparisons are reproduced graphically in Figs. 4c and d by simulations of ROSES spectra using the values of Table 1. There is extremely good agreement between the values of δ obtained using ROSES and MAT, as well as with the reference value. The value of the asymmetry

Table 1
^{13}C chemical sift anisotropy parameters for the carbonyl resonances of L-alanyl-L-aspartic acid

	CO Ala		$C_\gamma O$ Asp		CO Asp	
	δ (ppm)	η	δ (ppm)	η	δ (ppm)	η
Literature[a]	−81.5	0.86				
ROSES[b]	−81.0	0.85	82.5	0.70	−71.5	0.95
MAT[b]	−82.4	0.85	82.3	0.51	−71.7	0.80

Corresponding spectra are shown in Figs. 4b–d.
[a] From Ref. [35].
[b] Fits were done by manually comparing the experimental spectra of Fig. 4 with simulations. Experimental details are given in the text.

parameter determined by ROSES is also in very good agreement with the reference value for the CO-Ala site. There is a comparatively larger variation in the value of η determined using ROSES and MAT for all three sites. In this respect we remark that it is known that the determination of η from MAT type sideband patterns is known to be less accurate than the determination of δ [11], and that the accuracy deteriorates as the spinning speed is increased. We estimate the error on the measurement of η from these ROSES spectra with an effective spinning speed of 1.13 kHz to be around ± 0.1. It appears from the data in Table 1 that the asymmetry parameter is consistently slightly underestimated in the MAT data obtained at 2 kHz.

A visual appreciation of the data in Fig. 4 indicates that the centerband intensity seems to be weaker in the experimental spectra than predicted by the simulations. From Fig. 3, we also notice that the intensity of the centerband is at first sight the most important feature for the determination of the anisotropy parameter. Nevertheless, closer inspection shows that the asymmetry parameter is correlated to the relative intensities of the entire set of sidebands. Thus, as demonstrated by the fits to experiment (Fig. 4b), the asymmetry parameter for the CγO resonance is determined with good accuracy from the ROSES data. Other values of the asymmetry parameter give consistently worse fits.

Fig. 5 shows slices corresponding to the CH_3 resonance of the alanyl residue of the dipeptide in the ROSES experiment. Both spectra were obtained with a 15 kHz spinning speed using two different scaling factors (21 and 29.6). Fig. 6 shows data obtained with a ROSES experiment performed under exactly the same conditions as that of Fig. 5b, but with a powdered sample of 10 mg of the cyclic undecapeptide cyclosporin-A at natural abundance. These results show the applicability of the experiment to relatively large molecules presenting complex 1D spectra.

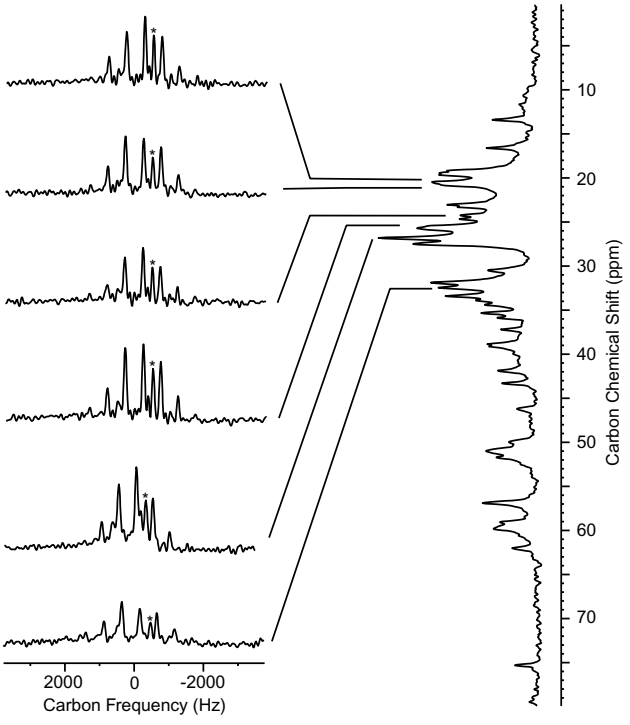

Fig. 6. F_1 traces extracted from the aliphatic region of a 2D ROSES spectrum of ~10 mg a powder sample of Cyclosporin-A. The spectrum on the right corresponds to the F_2 projection of the aliphatic region. Artefacts are indicated by asterisks. Two hundred and fifty-six scans were acquired for each of the 256 points in the t_1 dimension. Other experimental conditions were the same as for Fig. 5b.

6. Conclusion

A new 2D solid-state NMR experiment, which correlates fast (isotropic) and slow (anisotropic) spinning sideband patterns under fast MAS has been described for measuring CSA. An effective spinning speed ω_R/S is observed in the evolution dimension of the periodic rotor-synchronized ROSES experiment. Measurement of chemical shift anisotropy parameters is straightforwardly available from analysis of the spinning sideband intensities, which are different from those observed in standard slow magic-angle spinning experiments. Carbon-13 experiments involving spinning speed scaling factors as large as 30 were presented in this paper, which are by far the largest obtained to date. This type of experiment is therefore expected to be particularly useful for measurements of small chemical shift anisotropies, as is exemplified by the data presented for carbon resonances containing several observable sidebands even under 15 kHz spinning. The simplicity of the periodic unit of the ROSES sequence, which involves two π-pulses, leads us to believe that it is a promising candidate for adaptation to proton spectroscopy, in combination with homonuclear decoupling. Preliminary experiments on protons have been successfully performed on powder samples of small molecules, and we are currently pursuing these experiments.

Acknowledgments

The authors would like to thank Prof. Jay H. Baltisberger (Berea) for his insights into sideband patterns, and Dr. D. Sakellariou (Berkeley) for helpful discussions.

References

[1] I.J. Lowe, Phys. Rev. Lett. 2 (1959) 285–286.
[2] E.R. Andrew, E.L. Bradbury, R.G. Eades, Nature 183 (1959) 1802–1803.
[3] L. Emsley, D.D. Laws, A. Pines, in: B. Maraviglia (Ed.), Proceedings of the International School of Physics Enrico Fermi, Course CXXXIX, 1998.
[4] M. Hong, J. Am. Chem. Soc. 122 (2000) 3762–3770.
[5] M. Crozet, M. Chaussade, M. Bardet, L. Emsley, B. Lamotte, J.M. Mouesca, J. Phys. Chem. A 104 (2000) 9990–10000.
[6] Z.R. Wu, N. Tjandra, A. Bax, J. Am. Chem. Soc. 123 (2001) 3617–3618.
[7] D.M. Grant, Chemical Shift Tensors, A.M. Orendt, Chemical shift tensor measurement in solids, in: D.M. Grant, R.K. Harris (Eds.), Encyclopedia of Nuclear Magnetic Resonance, Wiley, Chichester, 1996.
[8] M.M. Maricq, J.S. Waugh, J. Chem. Phys. 70 (1979) 3300–3316.
[9] J. Herzfeld, A.E. Berger, J. Chem. Phys. 73 (1980) 6021–6030.
[10] J. Herzfeld, X. Chen, Sideband analysis in magic angle spinning NMR of solids, in: D.M. Grant, R.K. Harris (Eds.), Encyclopedia of Nuclear Magnetic Resonance, Wiley, Chichester, 1996.
[11] P. Hodgkinson, L. Emsley, J. Chem. Phys. 107 (1997) 4808–4816.
[12] Z.H. Gan, J. Am. Chem. Soc. 114 (1992) 8307–8309.
[13] J.Z. Hu, D.W. Alderman, C. Ye, R.J. Pugmire, D.M. Grant, J. Magn. Reson. A 105 (1993) 82–87.
[14] S.L. Gann, J.H. Baltisberger, A. Pines, Chem. Phys. Lett. 210 (1993) 405–410.
[15] W.T. Dixon, J. Magn. Reson. 44 (1981) 220–223.
[16] S. Féaux de Lacroix, J. Titman, A. Hagemeyer, H. Spiess, J. Magn. Reson. 97 (1992) 435–443.
[17] O.N. Antzutkin, S.C. Shekar, M.H. Levitt, J. Magn. Reson. Ser. A 115 (1995) 7–19.
[18] M.A. Alla, E.I. Kundla, E.T. Lippmaa, JETP Lett. 27 (1978) 194–197.
[19] R. Tycko, G. Dabbagh, P.A. Mirau, J. Magn. Reson. 85 (1989) 265–274.
[20] S-F. Liu, J-D. Mao, K. Schmidt-Rohr, J. Magn. Reson. 155 (2002) 15–28.
[21] A. Bax, N.M. Szeverenyi, G.E. Maciel, J. Magn. Reson. 55 (1983) 494–497.
[22] T. Terao, T. Fujii, T. Onodera, A. Saika, Chem. Phys. Lett. 107 (1984) 145–148.
[23] T.M. de Swiet, M. Tomaselli, A. Pines, Chem. Phys. Lett. 285 (1998) 59–63.
[24] A.C. Kolbert, D.P. Raleigh, M.H. Levitt, R.G. Griffin, J. Chem. Phys. 90 (2) (1989) 679–689.
[25] T. Gullion, J. Magn. Reson. 85 (1989) 614–619.
[26] C. Crockford, H. Geen, J. Titman, Chem. Phys. Lett. 344 (2001) 367–373.
[27] O.N. Antzutkin, Prog. Nucl. Magn. Res. 35 (1999) 203–266.
[28] M.E. Rose, Elementary Theory of Angular Momentum, Wiley, New York, 1967.
[29] M. Goldman, Quantum Description of High-Resolution NMR in Liquids, Oxford University Press, New York, 1988.
[30] E.T. Olejniczak, S. Vega, R.G. Griffin, J. Chem. Phys. 81 (1984) 4804–4817.
[31] M. Bak, J.T. Rasmussen, N.C. Nielsen, J. Magn. Reson. 147 (2000) 296–330.
[32] P. Hodgkinson, L. Emsley, Prog. Nucl. Magn. Reson. Spectrosc. 36 (2000) 201–239.
[33] M.H. Levitt, R. Freeman, J. Magn. Reson. 33 (1979) 473–476.
[34] D.J. States, R.A. Haberkorn, D.J. Ruben, J. Magn. Reson. 48 (1982) 286–292.
[35] Y. Wei, D-K. Lee, A. Ramamoorthy, J. Am. Chem. Soc. 123 (2001) 6118–6126.